HiLL PUBLISHING

Journal of Electrical Power & Energy Systems, 2023, 7(2), 81-91
https://www.hillpublisher.com/journals/jepes/
ISSN Online: 2576-053X
ISSN Print: 2576-0521

Winding Design and Lead-angle Control for the Maximum Speed of an Interior Permanent-Magnet Brushless DC Motor

Myongsong Cha*, Chol Sok, Chon Ung Kim

Department of Electrical Engineering, Kim Chaek University of Technology, Pyongyang, Democratic People's Republic of Korea.

How to cite this paper: Myongsong Cha, Chol Sok, Chon Ung Kim. (2023) Winding Design and Lead-angle Control for the Maximum Speed of an Interior Permanent-Magnet Brushless DC Motor. *Journal of Electrical Power & Energy Systems*, 7(2), 81-91.
DOI: 10.26855/jepes.2023.12.005

Received: November 28, 2023
Accepted: December 26, 2023
Published: January 23, 2024

***Corresponding author:** Myongsong Cha, Department of Electrical Engineering, Kim Chaek University of Technology, Pyongyang, Democratic People's Republic of Korea.

Abstract

This paper presents the winding design and lead angle control for the maximum speed of an Interior Permanent-Magnet Brushless DC Motor (IPMBLDCM) for the subway locomotive. The maximum speed of the IPMBLDCM is regulated by the linkage flux and armature reaction by lead angle control because permanent magnet magnetomotive force(mmf) cannot be regulated directly. The maximum speed of IPMBLDCM for the subway locomotive is 2.34 times than rated speed. As the speed regulation ratio is larger than 2, the maximum speed of the motor must be ensured by lead-angle and conductors per slot. If lead-angle is regulated, no-load speed is increased by linkage flux changing at the no-load state, and rated speed is increased by armature reaction. The relation between the speed and torque, output power, efficiency by lead angle, and conductors per slot are simulated in Ansoft Maxwell/RMxprt software. The simulation result verified that the speed and torque, output power, and efficiency are constant at the range of 47°~68° and the maximum speed is 1948r/min. Experimental results indicate that the operation of the IPMBLDCM considered is stable at the maximum speed.

Keywords

IPMBLDCM, Lead-angle control, linkage flux, armature reaction, maximum speed

1. Introduction

The IPMBLDCM without exciting winding and exciting source is widely used to replace the traditional DC motor for the subway locomotive. IPMBLDCM is gaining much interest in subway locomotive applications because of its high efficiency, simple control mode, and small size. The motor considered is a homemade 150kW, 3-phase, 8-pole IPMBLDCM. Its rated and maximum speeds are 835r/min and 1948r/min, respectively. PMBLDCM has a wide speed regulation range and start current and start torque, and the starting time is small [1, 2]. The torque ripple is reduced by dual mode coupling 120 conduction mode and 180 conduction mode in PMBLDCM [3, 4]. Also, PMBLDCM generates enough torque and speed by combining the mode of motor/generator [5]. From zero to base speed, it is dependent on applied voltage, and above the base speed, it is dependent on flux weakening by torque angle [6]. The armature reaction effect and winding inductance of PMBLDCM are analyzed in the FEM [7]. In [8, 9], the speed of PMBLDCM is regulated by voltage. In this case, the torque is constant and output power is increased with speed. In [10-20], maximum speed of PMBLDCM is regulated by flux-weakening. If PMSM is operated to

PMBLDCM, it can be operated at high efficiency [21-23]. The paper presents the linkage flux and no-load speed regulation principle by lead-angle. Also, the d-axis armature reaction mmf to decrease permanent magnet mmf is presented by lead angle. The relation between the speed and torque, output power, efficiency by lead-angle, and conductors per slot are simulated, and a stable lead-angle range is found in Ansoft Maxwell/RMxprt software. Through experiment, speed and output power are measured by lead-angle, and conductors per slot to operate maximum speed are verified.

2. Linkage flux decreasing by the lead-angle control

To increase the speed of IPMBLDCM, it can use voltage regulation first and flux-weakening control after that. If the lead angle of phase winding is regulated in IPMBLDCM, the linkage flux of winding can be regulated. Each phase of winding is conducted at a 120° electric angle and two-phase winding is always conducted. When air-gap flux field distribution is 150° trapezoidal waveform and lead-angle are 0, $\frac{\pi}{3}$, $\frac{\pi}{2}$, the winding linkage flux density of IPMBLDCM is shown in Fig. 1.

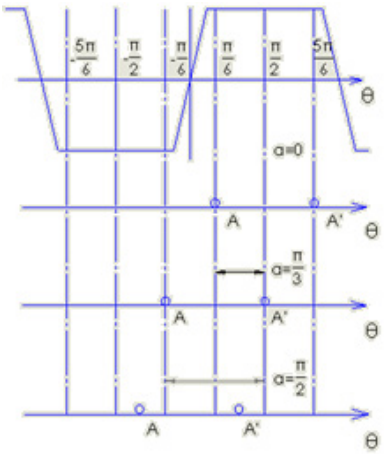

Figure 1. Winding linkage flux-density by the lead-angle.

Where θ is the electric angle and α is the lead-angle. The air-gap flux field distribution is 150° trapezoidal waveform in this paper. If lead angle is increased, the average linkage flux during conducting a range of 120° is decreased.

$$\begin{cases} \alpha = 0 & B = B_{\max} \\ 0 \le \alpha \le \frac{\pi}{3} & B = \left(-\frac{9}{2\pi^2}\alpha^2 + 1\right) B_{max} \\ \frac{\pi}{3} \le \alpha \le \frac{\pi}{2} & B = \left(-\frac{3}{\pi}\alpha + \frac{3}{2}\right) B_{\max} \end{cases} \tag{1}$$

$$\begin{cases} \alpha = 0 & \emptyset = BS = B_{\max} \quad S = \emptyset_0 \\ 0 \le \alpha \le \frac{\pi}{3} & \emptyset = \left(-\frac{9}{2\pi^2}\alpha^2 + 1\right) \emptyset_0 \\ \frac{2\pi}{3} \le \alpha \le \frac{\pi}{2} & \emptyset = \left(-\frac{3}{\pi}\alpha + \frac{3}{2}\right) \emptyset_0 \end{cases} \tag{2}$$

As known from equation (2), linkage flux by the lead-angle is decreased and flux-weakening effect appears.

3. No-load speed by the lead-angle

If back-emf induced in phase winding is constant, no-load speed by the lead-angle is obtained as

$$\begin{cases} \alpha = 0 & n_0 = n_N, \quad \emptyset = \emptyset_0, \quad E = C_e \emptyset_0 n_N \\ & 0 \le \alpha \le \frac{\pi}{3} \quad n_0 = \frac{n_N}{\left(-\frac{9}{2\pi^2}\alpha^2 + 1\right)} \\ & \frac{\pi}{3} \le \alpha \le \frac{\pi}{2} \quad n_0 = \frac{n_N}{\left(-\frac{3}{\pi}\alpha + \frac{3}{2}\right)} \end{cases} \tag{3}$$

From equation (3), it is known that no-load speed is increased when the lead angle is large. When the lead angle is 60°, the no-load speed is increased twice. If the lead angle is increased from 60° to 89°, no-load speed is increased quickly. When lead-angle is increased more than 84°, no-load speed is increased rapidly.

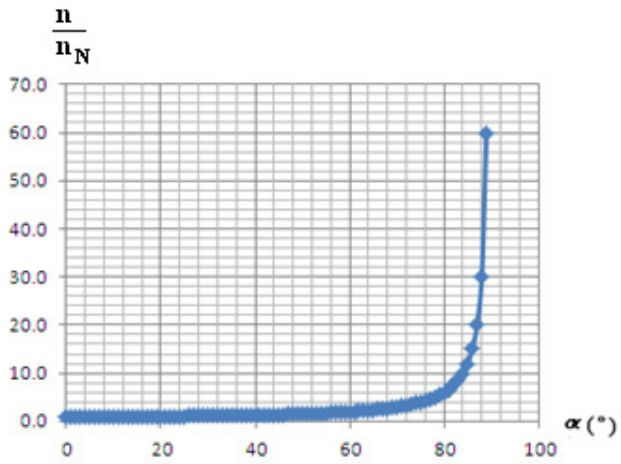

Figure 2. No-load speed by the lead-angle.

This is the theoretical analysis when air-gap flux field distribution is 120° trapezoidal waveform and the conducting angle of phase winding is 120°. When air-gap flux field distribution is a wide trapezoidal waveform than 120° and the lead-angle is controlled, circle current flows between the inverter and non-conducting winding, and it is generated damping torque. Therefore, maximum speed is verified correctly.

4. Average d-axis armature reaction mmf changing by the lead-angle

The d-axis armature reaction mmf is changed by lead-angleα.

1) lead-angle $\alpha = 0$

While the rotor pole of IPMBLDCM moves from the start position in Fig.3.1 to the end position in Fig.3.2, the A phase conducts in a positive direction, and the B phase conducts in a negative direction. The armature reaction mmf changes the amplitude and waveform of the air-gap flux field. Figure 3 shows the armature reaction mmf at lead-angle 0.

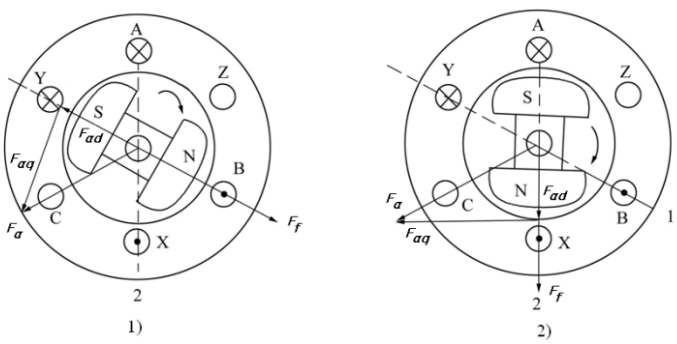

Figure 3. Armature reaction mm fat the lead-angle 0.

In Fig. 3, F_a is armature reaction mmf, F_{ad} is d-axis armature reaction mmf, $F_{aq}$is q-axis armature reaction mmf, F_f is permanent magnet mmf. The armature reaction mmf of one-phase winding is expressed by

$$F_{a1} = \frac{w \cdot k_{dp}}{2p} \cdot I \tag{4}$$

where w is the number of turns per phase, k_{dp} is the winding factor, I is the phase current. The resulting armature

reaction mmf for two phases can be obtained as

$$F_a = 2 \cdot F_{a1} \cdot \sin\frac{\pi}{3} = \sqrt{3} \cdot \frac{w \cdot k_{dp}}{2p} \cdot I \tag{5}$$

The d-axis armature reaction mmf does flux-weakening action at the start position and flux-strengthening action at the end position, therefore average d-axis armature reaction mmf does nothing.

2) lead-angle $\alpha = \frac{\pi}{6}$

Figure 4 shows the armature reaction mmf at lead-angle $\frac{\pi}{6}$. The relation between armature reaction mmf F_a and permanent magnet mmf at the start position is shown in Fig. 4(1).

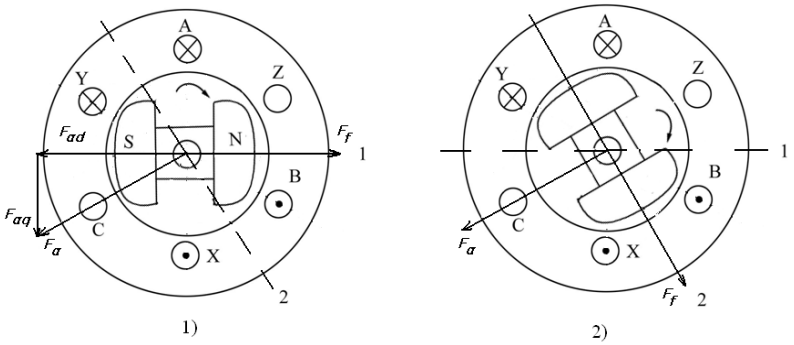

Figure 4. Armature reaction mmfat the lead-angle $\frac{\pi}{6}$.

At that time, F_a decreases F_f .

$$F_{ad1} = F_a cos\frac{\pi}{6} \tag{6}$$

The d-axis armature reaction mmf is not existed at the end position in Fig. 4(2).

$$F_{ad2}=0$$

The average d-axis armature reaction mmf is obtained as.

$$F_{adm} = \frac{1}{2}(F_{ad1} + F_{ad1}) = \frac{1}{2}F_a cos\frac{\pi}{6} \tag{7}$$

3) lead-angle $\alpha = \frac{\pi}{3}$

Figure 5 shows the armature reaction mmf at lead-angle $\frac{\pi}{3}$. All of the armature reaction mmf is the d-axis armature reaction mmf and do maximum flux-weakening action at the start position in Fig. 5(1).

$$F_{ad1} = F_a \tag{8}$$

The q-axis armature reaction mmf F_{aq} is not existed and electromagnetic torque is not generated.

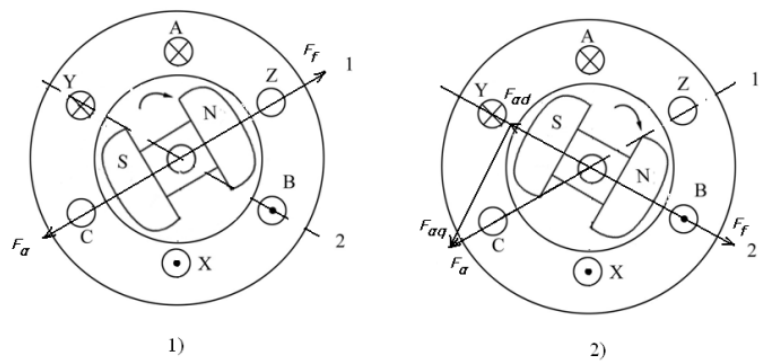

Figure 5. Armature reaction mmfat the lead-angle $\frac{\pi}{3}$.

The d-axis armature reaction mmf F_{ad} do flux-weakening actionat the end position in Fig. 5.2.

$$F_{ad2} = F_a cos\frac{\pi}{3} \tag{9}$$

Average d-axis armature reaction mmf is obtained as.

$$F_{adm} = \frac{1}{2}(F_{ad1} + F_{ad2}) = \frac{1}{2}F_a\left(1 + cos\frac{\pi}{3}\right) \tag{10}$$

4) lead-angle$\alpha = \frac{\pi}{2}$

The average d-axis armature reaction mmf is obtained as.

$$F_{adm} = \frac{1}{2}F_a\left(\cos\frac{\pi}{6} + \cos\frac{\pi}{6}\right) = F_a\cos\frac{\pi}{6} \tag{11}$$

The q-axis armature reaction mmf F_{aq} generates damping torque at the start position and rotating torque at the end position. Therefore, average rotating torque is not generated and IPMBLDCM is not operated. The results of the average d-axis armature reaction mmf by the lead angle are summarized in Table 1.

Table 1. Average d-axis armature reaction mmf by the lead-angle

№	Lead-angle	Average d-axis armature reaction mmf
1	0	0
2	$\frac{\pi}{6}$	$\frac{1}{2}F_a cos\frac{\pi}{6} = \frac{\sqrt{3}}{4}F_a$
3	$\frac{\pi}{3}$	$\frac{1}{2}F_a\left(1 + cos\frac{\pi}{3}\right) = \frac{3}{4}F_a$

The speed of IPMBLDCM is higher because the flux-weakening action of average d-axis armature reaction mmf is increased with lead-angle α. But the flux-weakening effect is less as the armature reaction mmf is much smaller than permanent magnet mmf.

5. Simulation result

The cross section of the home-made 150kW rated IPMBLDCM considered and its magnet pole structure is shown in Fig. 6. The rotor has the interior form, where the permanent magnet used is Nd-Fe-B. The stator has 48 slots and 48 coils.

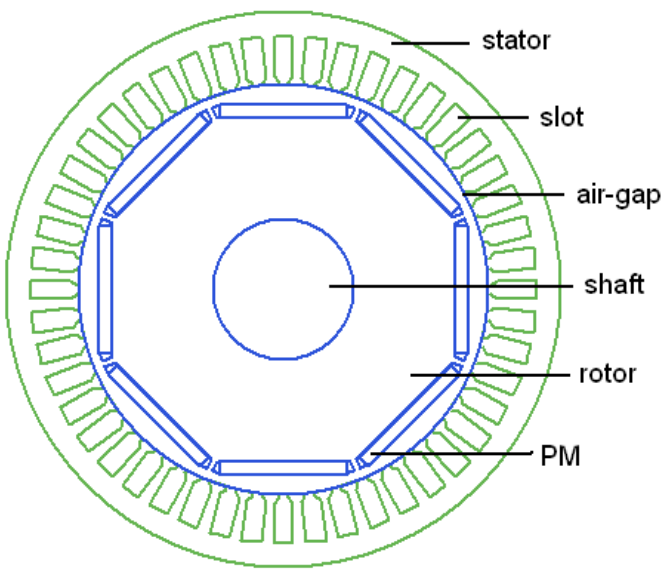

Figure 6. Cross section of the home-made 150kW rated IPMBLDCM.

The technical data for the 150kW IPMBLDCM considered is given in Table 2.

Table 2. IPMBLDCM data

No	Description	Dimension
1	Output power	150kW
2	Rated voltage	750V
3	Number of poles	8
4	Rated speed	835r/min
5	Maximum speed	1947r/min
6	Rated torque	1715Nm

The structural data for the 150kW IPMBLDCM considered is given in Table 3.

Table 3. Dimensions of the IPMBLDCM

No	Description	Dimension
1	Outer diameter of stator core	434mm
2	Inner diameter of stator core	323mm
3	Number of stator slot	48
4	Number of phase	3
5	Conductors per slot	8
6	Physical air gap	1mm
7	Core length	360mm
8	Magnet height	10mm
9	Magnet width	100mm

The simulation is done in ANSOFT MAXWELL/RMxprt software.
The flux field distribution of IPMBLDCM in the no-load state is shown in Fig. 7.

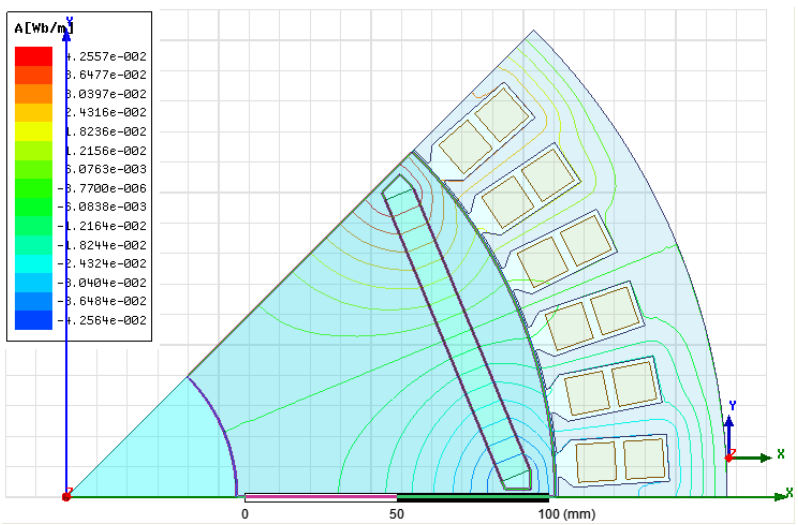

Figure 7. Flux field distribution in the no-load state.

Fig. 8 shows the no-load air-gap flux density distribution under one pole.
The no-load speed and rated speed, efficiency, torque, output power of 150kW IPMBLDCM is simulated by lead-

angle and different conductors per slot in Ansoft Maxwell/RMxprt software.

Fig. 9 shows the no-load speed curve by the lead-angle and conductors per slot.

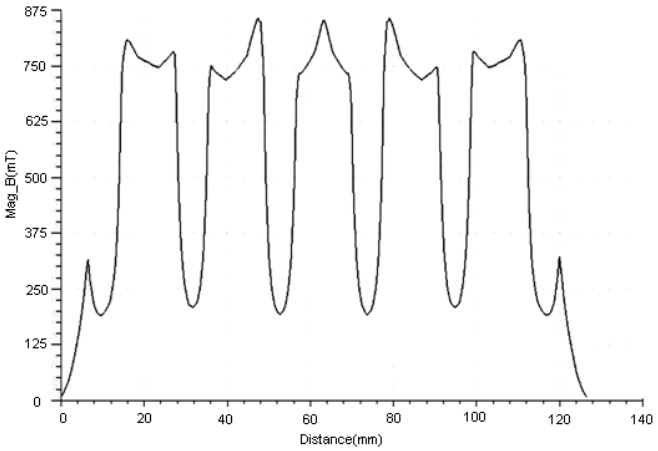

Figure 8. No-load air-gap flux density distribution under one pole.

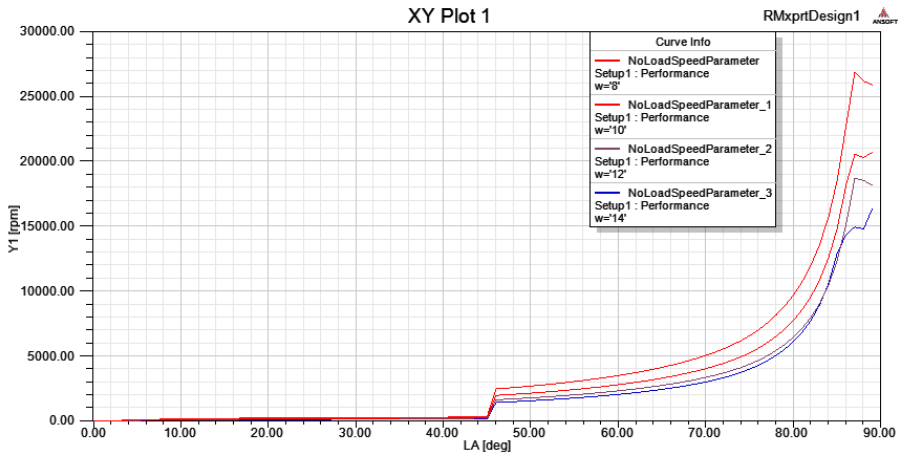

Figure 9. No-load speed curveby the lead-angle and conductors per slot.

As above theoretical analysis, the more lead-angle increases, the more quickly the no-load speed increases. Fig. 10 shows the rated speed curve by the lead angle and conductors per slot.

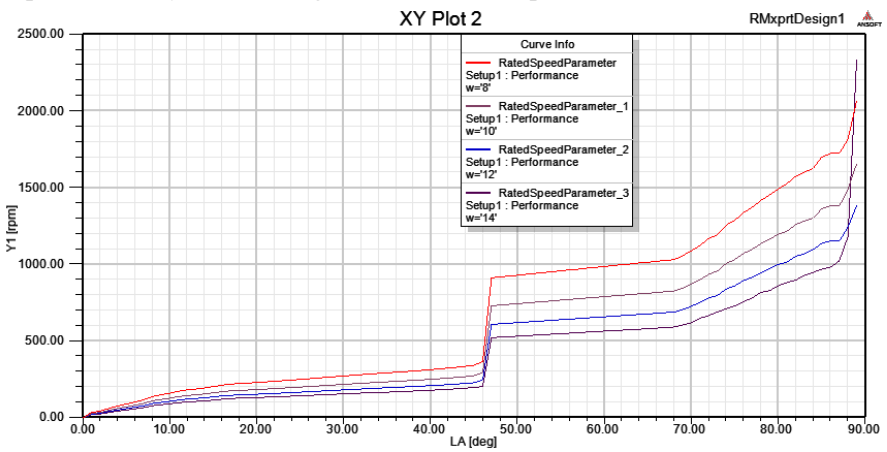

Figure 10. Rated speed curve by the lead-angle and conductors per slot.

When the lead angle is 47° and conductors per slot are 8, the rated speed is 835r/min and when the lead angle is 89° and conductors per slot are 8, the maximum speed is 1948r/min. When the conductors per slot are 10, 12, and 14, the rated and maximum speed is lower. Fig. 11 shows the efficiency curve by the lead angle and conductors per slot.

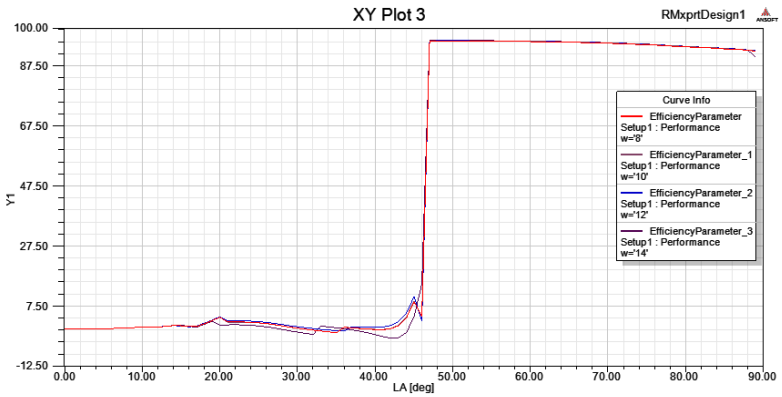

Figure 11. Efficiency curve by the lead-angle and conductors per slot.

The efficiency is between 95~92 percent when the lead angle is larger than 47°. Fig. 12 shows the output power curve by the lead angle and conductors per slot.

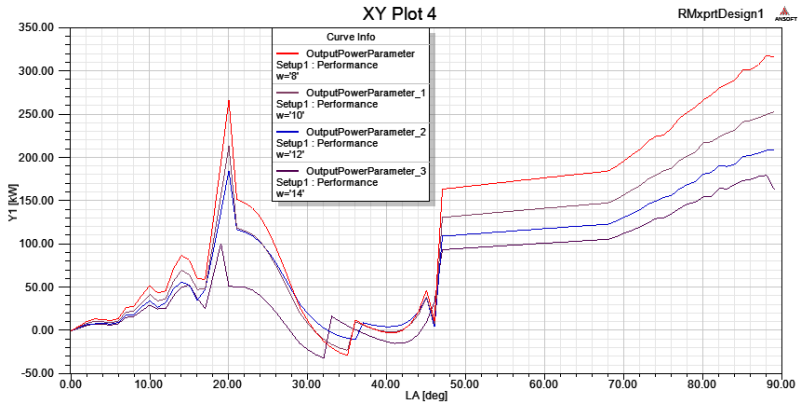

Figure 12. Output power the lead-angle and conductors per slot.

The output power is generated at 150kW when conductors per slot are 8, but the output power is lower than 150kW when conductors per slot are larger than 8. Fig. 13 shows the rated torque curve by the lead angle and conductors per slot.

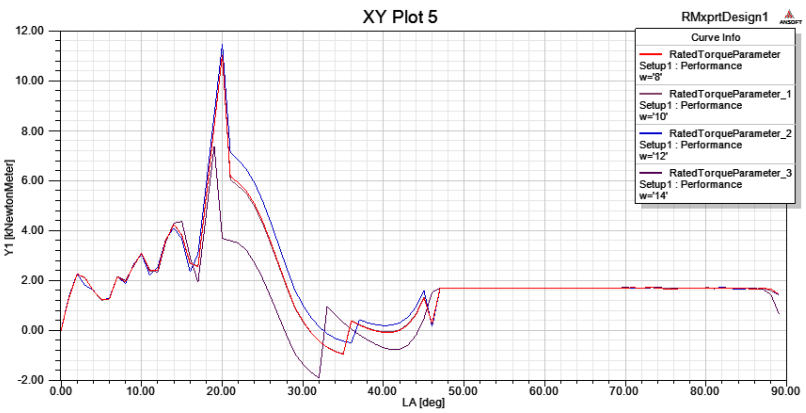

Figure 13. Rated torque curve by the lead-angle and conductors per slot.

Fig. 14 shows the efficiency and speed, rated torque, and output power curve by the lead-angle when conductors per slotare 8.

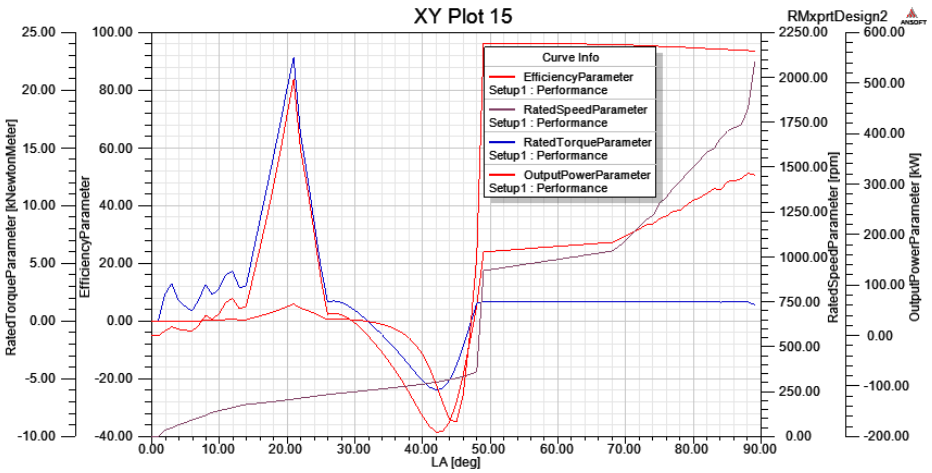

Figure 14. Relation between efficiency, speed, torque, output power.

To operate IPMBLDCM stable, motor property values must be constant at any range of lead-angle. The stable lead-angle range of IPMBLDCM is 47°~68° in Fig. 14.

6. Experimental results

The IPMBLDCM considered is shown in Fig. 15.

Figure 15. The IPMBLDCM.

The speed and torque, output power, efficiency are tested on the lead-angle control of 150kW, 3-phase, 8-pole IPMBLDCM. The characteristic are tested as the lead-angle changes from 0° to 89°.Experiment results are reported in Table 4.

Table 4. Experiment results

No	Lead-angle(°)	I(A)	P(kW)	n(r/min)	T(Nm)
1	49	260	150	835	1710
2	68	230	150	1030	1390
3	89	210	150	2080	705

The speed curve by the lead-angle of IPMBLDCM which is to be observed in the real experiment is shown in Fig. 16.

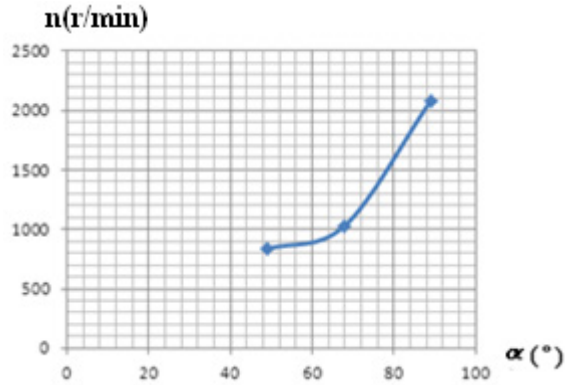

Figure 16. Speed curve by the lead-angle.

As can be seen from the experiment results, when the conductors per slot are 8 and the lead-angle is 88°, IPMBLDCM confirms to attain the rated speed of 835r/min and the maximum speed of 1948r/min with safety.

7. Conclusion

The linkage flux changing by lead-angle is increased no-load speed of IPMBLDCM. At the load state, the armature reaction does reflux-weakening action but its effect is small. The main flux-weakening effect is dependent on linkage flux by lead angle and the d-axis armature reaction effect is less. And linkage flux and d-axis armature reaction mmf are explained in the equation. The simulation result in Ansoft Maxwell/RMxprt software is verified rated and maximum speed and output power and stable operation range. The experiment result shows that the theoretical analysis and simulation results are correct.

References

[1] Ahmed M. Ahmed, Mohamed S. Elksasy, Amr Ali-Eldin, & Faiz F. Areed. Brushless DC Motor Speed Control Using Both PI Controller and Fuzzy PI Controller. International Journal of Computer Applications, Volume 109, No. 10, January 2015, 29-35.

[2] Ping Zheng, Yong Liu, Yan Wang, & Shukang Cheng. Magnetization Analysis of the Brushless DC Motor Used for Hybrid Electric Vehicle. IEEE Transactions on Magnetics, Vol. 41, No. 1, January 2005, 522-524.

[3] S.S. Bharatkar, R. Yanamshetti, D. Chatterjee, & A.K. Ganguli. Dual-Mode Switching Technique for Reduction of Commutation Torque Ripple of Brushless DC Motor, IET Electr. Power Appl., 2011, Vol. 5, 193-202.

[4] Yong Liu, Z. Q. Zhu, & David Howe. Direct Torque Control of Brushless DC Drives with Reduced Torque Ripple. IEEE Transactions on Industry Applications, Vol. 41, No. 2, March/April 2005, 599-608.

[5] I. Janpan, R. Chaisricharoen, & P. Boonyanant. Control of the Brushless DC Motor in Combine Mode. Procedia Engineering, 2012, Vol. 32, 279-285.

[6] D. M. Ionel, J. F. Eastham, T. J. E. Miller, & E. Demeter. Design Considerations for Permanent Magnet Synchronous Motors for Flux Weakening Applications. IEE Proc-Electr. Power Appl., Vol.145, No.5, September 1998, 435-440.

[7] Parag R. Upadhyay, K. R. Rajagopal, & B. P. Singh. Effect of Armature Reaction on the Performance of an Axial-Field Permanent-Magnet Brushless DC Motor Using FE Method. IEEE Transactions on Magnetics, Vol. 40, No. 4, July 2004, 2023-2025.

[8] Bhim Singh & Vashist Bist. A BL-CSC Converter-Fed BLDC Motor Drive with Power Factor Correction. IEEE Transactions on Industrial Electronics, Vol. 62, No. 1, January 2015, 172-183.

[9] Fabio Giulii Capponi, Roberto Terrigi, Federico Caricchi, & Luca Del Ferraro. Active Output Voltage Regulation for an Ironless Axial-Flux PM Automotive Alternator with Electromechanical Flux Weakening. IEEE Transactions on Industry Applications, Vol. 45, No. 5, September/October 2009, 1785-1793.

[10] Emine Bostanci, Zdeno Neuschl, & Robert Plikat. No-Load Performance Analysis of Brushless DC Machines with Axially Displaceable Rotor. IEEE Transactions on Industrial Electronics, Vol. 61, No. 4, April 2014.

[11] Keitaro Ueda, Shigeo Morimoto, Yukinori Inoue, & Masayuki Sanada. A Novel Control Method in Flux-weakening Region for Efficient Operation of Interior Permanent Magnet Synchronous Motor. IEEJ Journal of Industry Applications, Vol.4, No.5, 2015,

619-625.

[12] Gianmario Pellegrino, Eric Armando, & Paolo Guglielmi. Direct Flux Field-Oriented Control of IPM Drives with Variable DC Link in the Field-Weakening Region. IEEE Transactions on Industry Applications, Vol. 45, No. 5, September/October 2009, 1619-1627.

[13] Hong-xing Wu, Shu-kang Cheng, & Shu-mei Cui. A Controller of Brushless DC Motor for Electric Vehicle. IEEE Transactions on Magnetics, Vol. 41, No. 1, January 2005, 509-513.

[14] Yoshihiro Okuyama, Tomohiro Tanaka, Tsuyoshi Hanamoto, & Hiroaki Yamaga. A New Current Vector Control Method of IPMSM in Flux Weakening Region to Prevent Inverter Voltage Saturation. IEEJ Journal of Industry Applications, Vol.2, No.6, 2013, 315-322.

[15] Jiunn-Jiang Chen & Kan-Ping Chin. Automatic Flux-Weakening Control of Permanent Magnet Synchronous Motors Using a Reduced-Order Controller. IEEE Transactions on Power Electronics, Vol. 15, No. 5, September 2000, 881-890.

[16] Ayman M. EL-Refaie, Thomas M. Jahns, Patrick J. McCleer, & John W. McKeever. Experimental Verification of Optimal Flux Weakening in Surface PM Machines Using Concentrated Windings. IEEE Transactions on Industry Applications, Vol. 42, No. 2, March/April 2006, 443-453.

[17] Jiunn-Jiang Chen & Kan-Ping Chin. Minimum Copper Loss Flux-Weakening Control of Surface Mounted Permanent Magnet Synchronous Motors. IEEE Transactions on Power Electronics, Vol. 18, No. 4, July 2003, 929-936.

[18] M. Nasir Uddin & Md. Muminul Islam Chy. Online Parameter-Estimation-Based Speed Control of PM AC Motor Drive in Flux-Weakening Region. IEEE Transactions on Industry Applications, Vol. 44, No. 5, September/October 2008, 1486-1494.

[19] Ayman M. EL-Refaie, & Thomas M. Jahns. Optimal Flux Weakening in Surface PM Machines Using Fractional-Slot Concentrated Windings. IEEE Transactions on Industry Applications, Vol. 41, No. 3, May/June 2005, 790-800.

[20] Keiichiro Kondo & Satoshi Kitamura. Torque Control Method for Permanent Magnet Synchronous Motor Operating in Field Weakening Region at Middle Speed Range. IEEJ Journal of Industry Applications, Vol.2, No.2, 2013, 106-112.

[21] Z. Q. Zhu, J. X. Shen, & D. Howe. Flux-weakening Characteristics of Non-sinusoidal Back-EMF PM Machines in Brushless DC and AC Modes. Journal of Asian Electric Vehicles, volume 4, number 2, December 2006, 919-925.

[22] Masataka Miyamasu & Kan Akatsu. Efficiency Comparison between Brushless DC Motor and Brushless AC Motor Considering Driving Method and Machine Design. IEEJ Journal of Industry Applications, Vol.2, No.1, 2013, 79-86.

[23] Tingna Shi, Yuntao Guo, Peng Song, & Changliang Xia. A New Approach of Minimizing Commutation Torque Ripple for Brushless DC Motor Based on DC–DC Converter. IEEE Transactions on Industrial Electronics, Vol. 57, No. 10, October 2010, 3483-3490.